Hadronic correlation functions in the random instanton-dyon ensemble

Rasmus Larsen and Edward Shuryak

Department of Physics and Astronomy, Stony Brook University, Stony Brook, New York 11794-3800, USA

It is known since the 1980s that the instanton-induced 't Hooft effective Lagrangian not only can solve the so-called $U(1)a$ problem, by making the η' meson heavy etc., but it can also lead to chiral symmetry breaking. In the 1990s it was demonstrated that, taken to higher orders, this Lagrangian correctly reproduces effective forces in a large set of hadronic channels, mesonic and baryonic ones. Recent progress in understanding gauge topology at finite temperatures is related with the so-called *instanton-dyons*, the constituents of the instantons. Some of them, called L-dyons, possess the antiperiodic fermionic zero modes, and thus form a new version of the 't Hooft effective Lagrangian. This paper is our first study of a wide set of hadronic correlation function. We found that, at the lowest temperatures at which this approach is expected to be applicable, those may be well compatible with what is known about them based on phenomenological and lattice studies, provided L and M type dyons are strongly correlated.

I. INTRODUCTION

A. Instanton-dyons

Instantons are the 4-d topological solitons of the (Euclidean) gauge theory, discovered by Polyakov and collaborators [1]. The so-called instanton liquid model (ILM) has been proposed in [2]. Its main original application was related with explanation of chiral symmetry breaking, via collectivization of the so-called zero mode zone (or ZMZ for short). Another way to explain it is to state that the hypothetical 4-fermion interaction of the Nambu-Iona-Lasinio model [3] is in fact the instanton-induced 't Hooft Lagrangian. One may compare its two phenomenological parameters—the mean instanton size $\bar{\rho} \approx 1/3 fm$ and the total instanton-antiinstanton density $n \approx 1 fm^{-4}$—to two parameters of the NJL model, the coupling constant G and the cutoff Λ. Of course, the 't Hooft vertex does more than the NJL operator: in particular, it knows about chiral anomaly and correctly breaks the $U(1)_A$ symmetry. It also has a natural form factor, allowing to calculate diagrams of any order.

Further development, of the interacting instanton liquid model (IILM) in the 1990s has basically included the 't Hooft Lagrangian to all orders. The resulting theory was shown to reproduce well not only properties associated with the chiral symmetry breaking, the pions and their interactions, but also the correlation functions in such channels as vector and axial mesons, octet and decuplet baryons, and even glueballs, for a review see [4]. Among shortcomings of this theory is its inability to describe confinement.

The deconfinement order parameter, being nonzero at $T > T_c$, is the so called Polyakov line. Its vacuum expectation value $\langle P(T) \rangle \neq 0$ has been derived in multiple lattice works. It is interpreted as the appearance of the nonzero "holonomy field" $\langle A_4(T) \rangle \neq 0$. Modification of

the instanton solution to such environment has lead to the discovery of the KvBLL caloron solution [5,6] and realization that instantons can be disassembled into constituents, now called instanton-monopoles or instanton-dyons. They are allowed to have non-integer topological charge because they are connected only by (invisible) Dirac strings. Since these objects have nonzero electric and magnetic charges and source Abelian (diagonal) massless gluons, the corresponding ensemble is an "instanton-dyon plasma," with long-range Coulomb-like forces between constituents.

The first application of the instanton-dyons were made soon after their discovery in the context of supersymmetric gluodynamics [7]. This paper solved a puzzling mismatch of the value of the gluino condensate, between different answers obtained in various approaches. Diakonov and collaborators (for review see [8]) emphasized that, unlike the (topologically protected) instantons, the dyons are charged and thus interact directly with the Polyakov line. They suggested that since such dyon (anti-dyon) ensemble become denser at low temperatures, their backreaction may overcome the perturbative potential and drive it to its confining value, $\langle P \rangle \to 0$. A semiclassical confining regime has been defined by Poppitz *et al.* [9,10] in a carefully devised setting of softly broken supersymmetric models. While the setting includes a compactification on a small circle, with weak coupling and an *exponentially small* density of dyons, the minimum at the confining holonomy value is induced by the repulsive interaction in the dyon-antidyon molecules (called *bions* by these authors).

Recent progress to be discussed below is related to studies of the instanton-dyon ensembles. One series of papers were devoted to high-density phase and mean field approximation [11–15]. Our efforts were so far focused on the direct numerical simulation of the dyon ensembles [16–19]. These works had reproduced the deconfinement

and chiral restoration phase transitions, both in pure gauge [$SU(2)$] theory and in a QCD-like setting (2 colors and 2 light flavors). They also show strong modification of both transitions due to unusual quark periodicity phases [19].

Although in this paper we will be using $SU(3)$ color group, for simplicity let us start with the simplest case of the $SU(2)$. In the latter case there are only two self-dual (L and M) and two anti-self-dual ($\bar{L}$ and $\bar{M}$) instanton-dyon types. Their electric and magnetic charges make all combinations of ± 1. They form three distinct pairs LM, $L\bar{L}$, $L\bar{M}$ plus three conjugates, and the amount of screening depends on the effective interaction in each of them. Two obvious opposite limits are those of weakly correlated or random plasma, for which the mean field analysis would be adequate. Another limit is very strongly correlated ensemble. For example, if LM pairs be strongly correlated in their locations, their fields would be nearly vanishing: in fact this limit would return us to the "instanton liquid," in which the solitons are "neutral," without electric or magnetic charges. Strong correlation in the $L\bar{L}$ channel leads to vanishing magnetic, but not electric fields. Strong correlation in the last $L\bar{M}$ channel would on the contrary cancel electric but not magnetic charges.

Our previous studies were based on classical effective interaction derived from "streamline configurations" for last two channels $L\bar{L}$, $L\bar{M}$. The classical action in the instanton channel LM is different, it is "BPS protected", and so, at the classical level, no interaction was expected (or used in simulations). And yet, as we will show below, there are strong phenomenological evidences that even in this channel strong correlations of the instanton-dyons seem to be necessary.

By the present work we start a set of papers addressing some phenomenologically important issues of the instanton-dyon theory.

B. Hadronic correlation functions and structure of the QCD vacuum

Two-point correlation functions

$$K(x - y) = \langle J(x)J(y) \rangle \qquad (1)$$

of local gauge invariant operators J, to be referred as "currents" for brevity, are among the most fundamental observables of QCD. Since they are some functions of the distance between the two points $x_\mu - y_\mu$, one of the points can always be set to zero. In Euclidean thermal circle setting, there are two relevant variables, time separation $\tau = x_4 - y_4$ and distance $r = \sqrt{\sum_{m=1,2,3}(x_m - y_m)^2}$, and we will systematically put $r \to 0$, to focus inclusively on their τ dependence related to the energy spectrum of the theory.

The correlation functions are different for operators with different quantum numbers: for a general review of their phenomenology see [20]. Two-point correlations function, both for mesonic and baryonic operators, have been also has been calculated on the lattice, see, e.g., [21], and in the instanton liquid model (see review [4] and references therein).

Let us just remind few key facts. At large distances all correlation functions decrease exponentially, with the exponent given by the "spectral gap", the lowest excitation in the sector with the corresponding quantum numbers. Their opposite limit of small distances reflects propagation of the fundamental objects of the QCD, quarks and gluons. In between these two limits, one can compare the correlation functions to those of free propagation of quarks, and identify "attractive" and "repulsive" channels, being below or above the free propagation, respectively.

Specific combination of the two limits lead to successful parameterizations of the correlation functions, originally suggested in the context of the QCD sum rules [22]. The basic relation between the so called "spectral density", the imaginary part of the Fourier transform of the correlator in real time, and the real part of the correlator calculated in Euclidean time is given by the dispersion relation. Its coordinate form is

$$K(x, T) = \frac{1}{\pi} \int ds \, \mathrm{Im}\tilde{K}(s) D(\sqrt{s}, x, T) \qquad (2)$$

where the standard Mandelstam's invariant $s = -p^2$ is related with the Minkowskian momentum squared, and $D(M, x, T)$ is the Euclidean propagator of a particle of mass M to Euclidean distance x at temperature T.

Out of many possible quantum numbers, corresponding to various mesonic channels, we selected four most studied ones. Those are all for the "charged" isovector channels, say of $\bar{u}\Gamma d$ flavor structure, which does not require (statistically difficult) disconnected diagrams. The gamma matrices for the pseudoscalar P, vector V, axial vector A, and the scalar S correlators are

$$\Gamma = i\gamma_5, \gamma_0, \gamma_0\gamma_5, 1 \qquad (3)$$

respectively. The corresponding lowest mesonic states in these channels are the $\pi^-(134)$, $\rho^-(770)$, $a_1^-(1260)$, and the scalar $a_0^-(1450)$, the numbers are masses in MeV.

(In the literature on chiral symmetry breaking the isovector scalar channel—the $U(1)_a$ partner of the pion—is also known by its old name $\vec{\delta}$. Note also that the indicated state $a_0^-(1450)$ is the lowest $\bar{q}q$ meson state with this quantum number. The resonance $a_0(980)$ has near-degenerate isoscalar partner $f_0(980)$: those states are believed to be weakly bound mesonic molecules and thus are disregarded as far as the two-point correlator is concerned).

Since mesonic masses appear *squared* in the effective Lagrangians, consider approximate values of those for the channels under considerations,

$$m_{P,V,A,S}^2 \approx 0.02, 0.5, 1.58, 2.1 \text{ GeV}^2.$$

Two middle ones, the vector and axialvector, are the partners under the $SU(N_f)$ chiral symmetry, and their splitting in mass squared $m_A^2 - m_V^2 \approx 1$ GeV^2 indicate the strength of its breaking in the QCD vacuum. (In nonrelativistic quark model the vector is a "normal" meson, with the mass close to twice the constituent quark mass, and the axial vector is the orbital excitation.) The other two are the $U(1)_a$ chiral symmetry partners, and their squared masses are split more, by $m_S^2 - m_P^2 \approx 2$ GeV^2. To accommodate those in the nonrelativistic quark model one needs to include additional strong attraction/repulsion. As we will see below, all of these splittings are of the topological origin.

While the squared masses give some hints about the scale of $\bar{q}q$ interaction in these channels, much more detailed information on that comes from studies of the corresponding correlation functions. Theory and phenomenology of those, first systematically reviewed in [20], do indeed reveal very different x-dependence, depending on the quantum number of J. Some channels are "strongly attractive," with $K(x)$ exceeding the $K_0 \sim 1/x^6$ (corresponding to propagating massless quark and antiquark). Some are "strongly repulsive," while all vector channels (ρ, ω, ϕ) are "near-free," in the sense that $K(x)/K_0(x) \approx 1$ in a wide range. It is those splittings of the correlation functions $K(x)$ which we are going to calculate and discuss in this work.

A wider issue related to splittings of these functions is the spin-flavor structure of the nonperturbative effects in the QCD vacuum, leading to spontaneous breaking of the $SU(N_f)$ and explicit breaking of the $U(1)_a$ symmetry. The former issue we will study focusing on the *difference* between the vector and axial (isovector) correlation functions, $V - A$ for short. The latter one is related with the splitting between the pseudoscalar and scalar (isovector) correlation functions, $P - S$.

The $V \pm A$ combinations of the correlation functions are especially valuable. First of all, they can be deduced directly from experimental data, with good (few percent) accuracy. The vector ones have the spectral densities directly measurable via reaction $e^+e^- \to hadrons$. The axial ones are amenable via weak decays, most prominently of the reaction $\tau \to \nu_\tau + hadrons$. ALEPH collaboration data [23,24] remain the best one, used in both instanton study [25] and recently in the lattice calculation Ref. [26].

From the theoretical point of view, the best for our purposes is the *difference* $V - A$ of the vector and axial correlators. Due to chiral symmetry, pQCD diagrams with any number of exchanged gluons contribute equally to both of them, and are canceled in the difference. What remains are only the nonperturbative chiral symmetry breaking effects, which we focus on. We will specifically use $V - A$ combination of correlators below to determine the key parameter of the instanton-dyon ensemble.
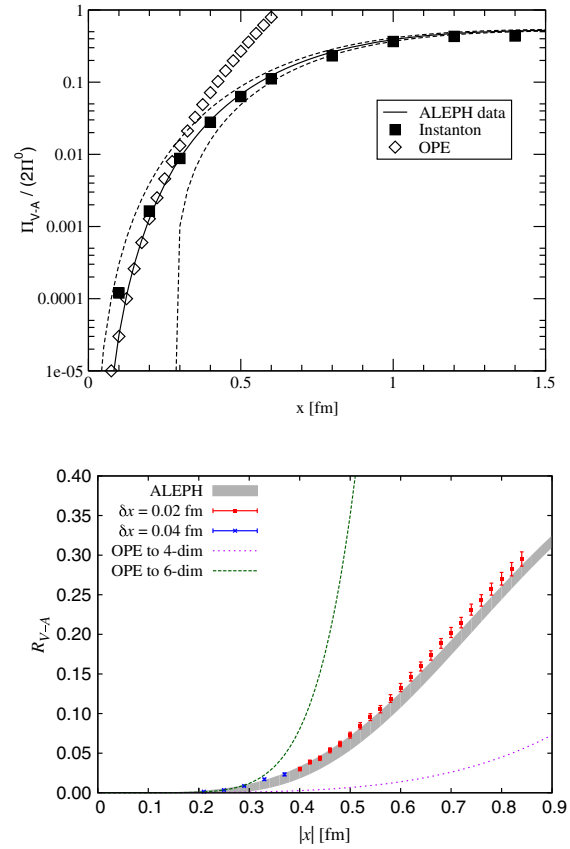

FIG. 1. $V - A$ correlation function as a function of the Euclidean distance x. The upper figure, from [25], compares the ALEPH data (region between two dashed lines) to the instanton liquid calculation (closed squares) and the OPE [22] (open rhombs). The lower plot, from [26], compares the same ALEPH data (shaded region) with versions of the OPE (lines) and to extrapolated results of their lattice simulations (red points).

In Fig. 1 we show the $V - A$ combination of correlators deduced from experimental ALEPH results, the instanton liquid calculation [25] (upper plot) as well as from the recent lattice study [26] (lower plot). Unlike older studies of point-to-point correlators, this one is done with dynamical quarks at physical mass, with proper continuum extrapolation. As one can see, both the ALEPH data and modern lattice do provide the correlation function with the accuracy of just a couple percents. Also it is evident from those plots that the original sum rule predictions [22] based on the operator product expansion (OPE) are applicable only at very small distances.

The strongest splitting of the correlation function, between the isovector pseudoscalar (charged $\vec{\pi}$) channel and the scalar (charged $\vec{\delta}$), reveals a very important feature of the QCD vacuum/matter structure, namely its *strong inhomogeneity*, but it reveals direct relation to *underlying topology* of the gauge fields. Unfortunately it is not so accurately known.

At small x the nonperturbative corrections to correlators—the splittings—are approximately given by expectation

values of $\langle J^2 \rangle$, or the *fluctuations* of the currents in the vacuum. In a bit more general terms, those are related to VEVs of various 4-fermion operators. Strong inhomogeneity of vacuum configurations means that those fluctuate from point to point by orders of magnitude. "Strong" feature can also be expressed as a statement that some VEVs are large

$$\langle O_{4-fermion} \rangle \gg \langle \bar{q}q \rangle^2$$

compared to the *quark condensate squared* in the r.h.s. There are plenty of the 4-fermion operators one can construct out of quark fields, and one may ask which ones show this feature in the most pronounced way. The studies, in the instanton framework [4] and in lattice simulations [27] concluded that it is (parts of) the topology-induced 't Hooft effective Lagrangian. For two light flavors its structure is

$$O_{4-fermion} \sim (\bar{u}_R \Gamma_i u_L)(\bar{d}_R \Gamma_i d_L) + (L \leftrightarrow R) \qquad (4)$$

where L, R are left and right handed components of the quark fields and Γ_i may include some color and Dirac matrices. This observation directly implies the presence of some small-size topological objects in the vacuum. Strongly enhanced local violation of $U(1)_a$ chiral symmetry was the key prediction of the "instanton liquid model," in which the typical instanton size is $\rho \sim 1/3\,fm$. The magnitude of the enhancement is inverse to the "diluteness fraction" of that model, the fraction of the 4-volume occupied by instantons $\sim (\rho/R)^4 \sim 1/3^4$.

C. The goals and structure of this paper

As we already mentioned above, the modern version of the semiclassical theory at temperatures comparable to the critical one is based not on instantons themselves, but on ensemble of their constituents, the instanton-dyons. Those came into existence due to inclusion of the nonzero VEV of the Polyakov line, also known as the "holonomy Higgsing." So far its trust was focused on the deconfinement and chiral phase transitions. Now we know that both of them can be reproduced by it, it is time to focus on the applicability limits of this theory, and see whether it does or does not reproduce correctly known effects as the theory approaches its boundary.

Without much details, let us state what is known about the limits of its applicability. The upper boundary is expected to be around $T \sim (2–3)T_c \sim 300–400$ MeV, where the Polyakov line VEV gets trivial $\langle P \rangle \to 1$. At higher temperatures the L-type dyons basically become the instantons themselves, while the M type dyons disappear.

Our attention in this work is focused on the lowest temperatures at which the instanton-dyon approach is expected to be applicable. It is clear that at $T \to 0$ it cannot be used, with the dyons being basically the 3-d solitons, and with their properties all normalized to T. As we detail below, at low T interference between the dyon fields do

lead to approximately 4-d spherically symmetric instantons, but these interferences are complicated.

The main question we try to answer in this work is whether the instanton-dyon ensemble can correctly reproduce the known features of hadronic correlation functions. It would be nice to have lattice data on the correlators as a function of the temperature: yet so far we only know them quantitatively at $T = 0$, in the QCD vacuum. Below we use the instanton-dyon model at its lowest edge, at the temperature $T = 100$ MeV, and compare the results with vacuum correlators.

In Sec. II we briefly outline general properties of dyons in $SU(3)$ and the random ensemble used in this paper.

In Sec. III we discuss the properties of the fermionic zero modes of the dyons. For the usual fermionic (antiperiodic in Matsubara time) quarks only one type of N_c dyons, called L dyon, has the fermionic zero modes. So, naively, in observables related with light quarks, such as the quark condensate, one should only consider subensemble of L dyons and forget about all M. However, we will show below that such approach cannot be used, because in fact those zero modes turn out to be extremely sensitive to LM correlations, Close proximity of M dyon to L can change local density of the zero modes by up to two orders of magnitude. We give the formula for the used approximations, the size of the box, amount of L dyons etc.,

In Sec. V we present and discuss our results for the mesonic and baryonic correlation functions. We start by showing the sensitivity of the correlators to LM correlations. We then tune the main parameter of the model r_{LM} to the best known $V - A$ combination of the correlation functions. After that, we present various other correlators. We obviously start with the strongest effect, the $U(1)a$ chiral symmetry breaking revealed in the $\vec{\pi} - \vec{\delta}$ splitting. (The vectors here stand for isovectors of the $N_f = 2$ theory.) At the end we present and discuss the resulting correlators for the Nucleon and Delta baryonic currents, and discuss strong attraction in the "good diquark" channel.

We summarize the paper in Sec. VI.

II. RANDOM ENSEMBLE IN SU(3)

Before we discuss the setting we use for our calculations, it is useful to recall the limitations of the semiclassical instanton-dyon theory.

At high T it is limited to the region in which the VEV of the Polyakov line is not too close to the unit value. The reason for that is that when the holonomy parameter ν is small, the M-type dyons become too light (and too large) to keep their semiclassical theory meaningful. In QCD this range approximately correspond to $T < 350$ MeV.

At low $T < T_c$, in the confined and chirally broken hadronic phase, the holonomy parameter ν is fixed to the confining value, so that $\langle P \rangle = 0$ and all types of dyons have the same actions. Yet as one moves toward the lower

temperatures, the action per dyon $S \sim 1/g^2(T)$ logarithmically decreases due to the running coupling, eventually making their semiclassical theory inapplicable. Tentatively we use as the lower "large" value $S_{M,L} \sim 3\hbar$. In QCD this range approximately correspond to $T > 100$ MeV

(Note that coincidentally this range correspond well to the temperature range of excited matter produced in heavy ion collisions at RHIC and LHC colliders).

In this first paper devoted to hadronic correlation functions we decided to use the simplest ensemble possible, in which positions and color orientations of the dyons are selected randomly. We will thus refer to this ensemble as random instanton-dyon model, or RIDM.

While our previous works used the simplest $SU(2)$ color group, we now switch to the $SU(3)$. Therefore we should start by defining the holonomy parametrization used. Standard holonomy phases μ_i, $i = 1..N_c$ should satisfy the zero-trace condition $\sum \mu_i = 0$. In addition, we assume that $\langle P \rangle$ is real. These two conditions reduce 3 phases to one free parameter

$$\mu_1 = 0, \qquad \mu_2 = -\mu_3 = \nu \qquad (5)$$

in terms of which VEV of the Polyakov line is

$$\langle P \rangle = \frac{1}{3} + \frac{2}{3}\cos(2\pi\nu). \qquad (6)$$

The confining value, at which it vanishes, is thus $\nu = 1/3$.

With this definition the actions of M_i, $i = 1, 2$ dyons are $S_M = S_0\nu$, where the instanton action $S_0 = 8\pi^2/g^2(T)$. The action of the "twisted" L-dyon is $S_L = S_0(1 - 2\nu)$. In the confining phase all of them have the same action $S_0/3$ and locations of three holonomy eigenvalues are as shown in Fig. 2, by blue circles.

III. FERMIONIC ZERO-MODES FOR CORRELATED $L - M$ DYONS

Zero-eigenstates of the Dirac operator play the central role in our calculation, as they provide the basic set of wave functions for the region in eigenvalues called the zero mode zone (or ZMZ for short) inside which the long-distance part of quark propagators is calculated. So, before we embark on modeling quark propagators and hadronic correlation functions, a direct comparison between those would be instructive.

We will subsequently discuss three historic approximations:

  (i) the original periodic instanton (caloron) at *zero* holonomy
  (ii) the single instanton-dyon (of the L type)
  (iii) the KvBLL caloron at *nonzero* holonomy, or the case of a set of interfering L, M_i dyons

Furthermore, since in a random ensemble of the instanton-dyons there are both self-dual and anti-self-dual objects,

there are no general formulas for these influences anyway. The practical solution we therefore use is to take as a basis the zero modes of the individual dyons.

The detailed derivation of those has been done in the appendix of [28]. Since it was done for arbitrary periodicity phase, it includes discussion of the delocalization of zero modes, at the values when color holonomy and flavor holonomy values coincide. Here we only need the zero mode for the physical antiperiodic quark fields, which for the L-type dyons has the following form

$$\phi_a^A = e^{i\pi t}\sqrt{\frac{\bar{v}^3}{2\pi}}\frac{\tanh(\bar{v}r/2)}{\sqrt{\bar{v}r\sinh(\bar{v}r)}}\epsilon_{aA}. \qquad (7)$$

Here and below in this section we write everything in units $T = 1$.. The normalization constant corresponds to $\int d^4x \text{Tr}[\phi\phi^*] = 1$.

The quark zero modes for the finite-T instantons, known as "calorons," are also known. Their gauge potential belongs to a general ansatz

$$A_\mu^a = \bar{\eta}_{\mu\nu}^a \Pi(x)\partial_\nu \Pi^{-1}(x) \qquad (8)$$

which in this case takes the form

$$\Pi(x) = 1 + \frac{\pi\rho^2 T}{r}\frac{\sinh(2\pi Tr)}{\cosh(2\pi Tr) - \cos(2\pi T\tau)} \qquad (9)$$

where ρ denotes the size of the instanton. Note that the dependence on Euclidean time τ is periodic, with the correct period $1/T$.

The fermion zero mode is also expressed in terms of this function

$$\psi_i^a = \frac{1}{2\sqrt{2}\pi\rho}\sqrt{\Pi(x)}\partial_\mu\left(\frac{\Phi(x)}{\Pi(x)}\right)\left(\frac{1 - \gamma_5}{2}\gamma_\mu\right)_{ij}\epsilon_{aj}, \qquad (10)$$

where

$$\Phi(x) = (\Pi(x) - 1)\frac{\cos(\pi T\tau)}{\cosh(\pi Tr)}.$$

Before we are going to compare these functions in more detail, it is instructive to compare their asymptotic behavior at large r. Both decay exponentially at large distances, but with different exponents. The L-dyon mode (7) decreases as $\exp(-\bar{v}r/2)$ prescribed by the magnitude of the corresponding holonomy. The caloron zero-mode (10) exponential decay is $\exp(-\pi r)$, related to the lowest fermionic Matsubara frequency. The two match only at high T where $\bar{v} \to 2\pi$.

So, already from the comparison of the asymptotic of these modes, one can preview the generic phenomenon: the sizes of the instanton-dyons in general (and their zero modes in particular) are *larger* than those of the calorons.
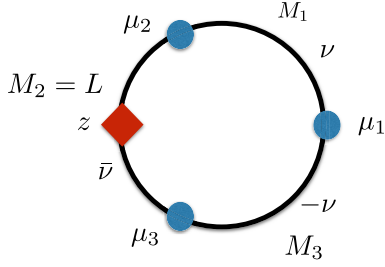
FIG. 2. The so called holonomy circle explaining notations used. Three blue points marked μ_1, μ_2, μ_3 correspond to three eigenvalues of the Polyakov line in $SU(3)$ gauge theory. Three sectors between those, marked M_1, $M_2 = L$, M_3 correspond to actions of the three types of the dyons. The red rhomb marked z corresponds to periodicity phase of the antiperiodic quarks: the sector containing it is the one which has the fermionic zero mode.

This statement may appear very counterintuitive, since the instanton-dyons are the caloron constituents. Note however, that interference of the instanton-dyon fields is mostly *destructive*.

Note also, that since at the higher-T limit of the instanton-dyon theory $\bar{\nu} \to 1$, in this limit the zero mode asymptotics for the L-dyon and the instanton match.

The size of the zero mode is also determined by the size parameter of the caloron ρ. At high $T > T_c$ temperatures the instanton density is corrected by the so called Pisarski-Yaffe factor which with a good accuracy is just the result of electric Debye screening by quarks and gluons scattering on the caloron

$$n_{\text{inst}}(T,\rho) = n_{\text{inst}}(0,\rho)e^{-\left(\frac{\rho}{\rho_T}\right)^2}$$
$$\frac{1}{\rho_T^2} = \frac{2N_c + N_f}{3}\pi^2 T^2 \qquad (11)$$

which forces the instanton sizes to scale with temperature like $\rho \sim \rho_T \sim 1/T$. (For explanations see, e.g., the review Schafer:1996wv.) However at small $T \to 0$ the instanton sizes have a constant limit, in the original instanton liquid model $\rho(T \ll T_c) \approx 1/3fm$. For QCD ($N_c = N_f = 3$) ρ_T reaches this value at $T = T_{\min} \approx 100$ MeV.

The main difference between the zero mode of the caloron and the L-dyon is that the former is strongly time-dependent. Substituting three different values of the size we see, from Fig. 3, that the density of the zero mode as a function of time changes by up to two orders of magnitude when $\rho = \rho_T$, but is weakly time dependent when $\rho = 1$ (that is $1/T$ in absolute units).

The space dependence of the caloron zero mode density is shown in Fig. 4. Here we compare the integrand of the normalization condition, thus multiply the densities by r^2. Note further that there are two dyon curves, corresponding to confining value $\bar{v} = 2\pi/3$ (valid at $T < T_c$) and the "trivial holonomy" value $\bar{v} = 2\pi$ valid at high T. Comparison of the plots indicate that while the ensemble
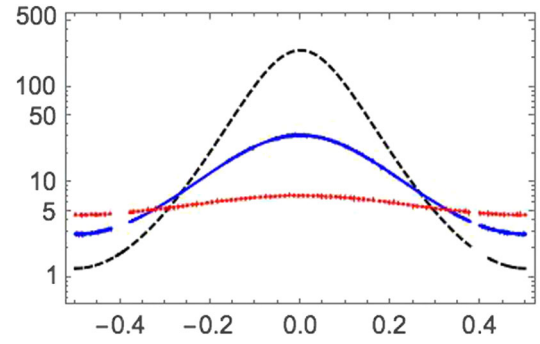

FIG. 3. The dependence of the caloron zero mode density on time, for $\rho = \rho_T$ (black dashed), $\rho = 2\rho_T$ (blue solid), and $\rho = 1$ (red dotted) lines. The quantity ρ_T is defined in (11).

of the calorons can be relatively dilute, that of the dyons cannot be such, because their zero modes have significantly larger range in space.

A popular measure of how strongly the function is localized is the integral of the density *squared*, or the 4th power of the zero mode

$$I_4 = \int d^4x [\text{Tr}(\phi\phi^+)]^2. \qquad (12)$$

(Let us recall that the integral of the second power is the normalization integral taken to be 1, and that the 4-fermion
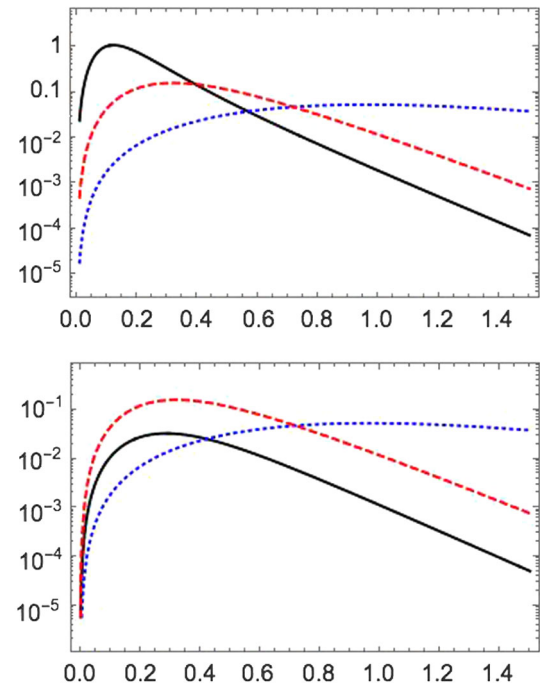

FIG. 4. The dependence of the zero mode densities times r^2 on r, for $t = 0$ (upper plot) and $t = 1/2$ (lower plot). Mote that these times correspond to the maximum and minimum in the previous plot. In all of them black solid curve is for the caloron with $\rho = \rho_T$, while blue dotted and red dashed curves are for the L-dyon, with $\bar{v} = 2\pi/3$ and 2π respectively.
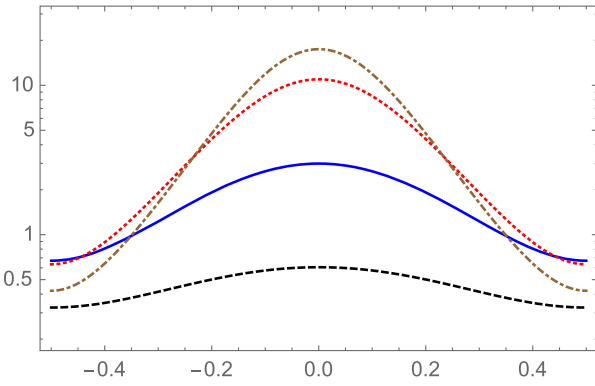
FIG. 5.   The time dependence of the zero mode densities, at $r = 0$, for the SU(2) caloron at confining holonomy $v = \bar{v} = \pi$. The lowest (black dashed) curve is at relative distance 1, the next (blue solid) is 0.5, then (red dots) 0.2 and (brown dash-dotted) one 0.1. The time and distances are in units such that $\beta = 1/T = 1$.

operator—'t Hooft effective Lagrangian—is instrumental in breaking the chiral symmetry).

For the caloron radii $\rho = \rho_T,\, 2\rho_T,\, 1$ (the same as shown in Fig. 3) its values are $I_4 = 26.6,\, 4.20,\, 1.55$, respectively.

All these comparisons suggest the inevitable conclusion: in distinction to the "instanton liquid"—which is relatively dilute, with the instantons occupying only few percent of the volume [2]—the ensemble of the instanton-dyons at $T < T_c$ is in fact rather dense.

Finally, we discuss the fermionic zero mode for a KvBLL caloron at *nonzero* holonomy worked out by van Baal and collaborators [29], using general ADHM and Nahm construction. That resulted in very complicated expressions which we do not copy here. The effect we are after takes into account mutual influence of the fields of L and M instanton-dyons, as a function of their relative distance, related to the "caloron size" parameter ρ via

$$r_{LM} = |\vec{r}_L - \vec{r}_M| = \pi\rho^2 T. \qquad (13)$$

The results are shown in Fig. 5: one can see that if the distance between the dyons is as large as 1 (the lowest black dashed curve), the time dependence is rather mild, resembling the infinite distance (single dyon) case discussed above, in which there is *no* t-dependence at all. But, as L and M are moved closer to each other, their interference deform the zero mode to be well localized. Indeed, close $L - M$ dyon pair is a small dipole, with electric and magnetic fields canceling outside. So the fermionic zero mode get strongly localized in between them.

The density of the zero modes can be written in a nice form (see, e.g., (11) of [29])

$$\hat{\Psi}_z^a(x)^+ \hat{\Psi}_z^b(x) = -\frac{1}{(2\pi)^2} \partial_\mu^2 \hat{f}_x^{ab}(z,z) \qquad (14)$$

where the r.h.s. is the Green function of certain equation in Nahm variable z.

A. The gauge factors of the zero-modes

Since we treat the dyons as individual object and do not include overlap effects, the dyon is an $SU(2)$ object. Higher order groups are obtained my taking the $SU(2)$ object and injecting it into a higher group, which in this case is the $SU(3)$.

To have more than one dyon in the same gauge, the hedgehog gauge dyon is rotated into a specific direction in color space. As in earlier work we choose to rotate the dyons into the τ_3 direction. In order to do this we first rotate all directions by an angle of ϕ around the τ_3, followed by a rotation of θ or $\pi - \theta$ for dyons and antidyons around the τ_2 direction, putting the direction along the z-axis corresponding to the τ_3 axis. Since any rotation around the z-axis in the xy plane will be invariant, we have a free rotation, corresponding to the $U(1)$ rotation. This angle sets the angle of the core and is important when dyons overlap each other. We therefore use the time coordinate for this rotation.

IV. THE SETTINGS

In our previous simulations [17,18] in the partition function the classical and one loop interactions of all dyon pair channels were included. The color group was $SU(2)$, and the 3-d manifold on which simulation was done was the 3d sphere S^3.

The instanton-dyons we use in this paper are embedded in $SU(3)$ color group. It has L, M_1, M_2 and their anti-solitons, 6 species in total. The 4-d manifold is the standard periodic Matsubara box, with variable space and time dimensions. The number of the dyons in the simulation we keep constant, $N_i = 100$, where i can be L or $\bar{L}$.

Since we only consider antiperiodic (fermionic) quarks, only the L, $\bar{L}$ dyons have quark zero modes. Thus the total basis of the zero mode zone is $N_L + N_{\bar{L}} = 200$ states. The propagation of quarks from one object to another is done via the "hopping matrix" T_{ij}, in this case the matrix of 200×200 size. Other dyons M_i only enter via their correlation/overlaps with L, $\bar{L}$, which we describe approximately via the parameter r_{LM} as detailed below.

The temperature has been set by the size of the box in temporal direction, which was chosen to be $2fm$, while the size of spatial directions was used to control the density. The density was found by fitting to experimental data as shown in section V.

The full zero-mode in $SU(2)$ and $SU(3)$ are known, but it is a huge expression which, even after long simplifications in Mathematica, is not viable to write in reasonably compact form. We have therefore generated numerically a set of graphs for their density distribution in space-time x and parametrized those approximately.

The zero-mode is a function of position x, holonomy ν and distance to the M dyon r_{LM}. We were interested in the shape for this at $\nu = 1/3$ and for distances $r_{LM} < 2$ for which the approximation works reasonably fine.

The form is

$$\psi_A^a = N\sqrt{f}\epsilon_{aA}$$

$$
\begin{aligned}
f \approx \exp[&(0.4 + \pi\exp[-4r_{LM}])(\cos[2\pi t] - 1)] \\
&\times 1/\cosh\left[-(\pi + (2\cos[\theta] + 10)\exp[-2r_{LM}])\right. \\
&\left.\times\sqrt{x^2 + y^2 + (z + 0.4r_{LM}^2)^2}]2\nu T\right],
\end{aligned}
\tag{15}
$$

where N is a normalization factor, since the parametrization normalization was slight of 1, θ is the angle between the L dyon to the M dyon and the position of the field. The color structure is given by the ϵ symbol.

The so-called hopping matrix is made of overlap matrix elements of the Dirac operator, symbolically

$$T_{ij} = \langle i|\hat{D}_\mu\gamma_\mu|j\rangle. \tag{16}$$

Here D_μ is the covariant derivative including the gauge field. If the fields is approximated by a sum of fields for each dyon, one can use Dirac equation of the zero mode to remove all fields and keep only the usual derivative. Those integrals were also numerically calculated and parametrized as follows

$$
\begin{aligned}
T_{ij} \approx \exp\left[-\sqrt{0.7 + (2\pi(\nu/2 + \bar{\nu}/2.5\exp[-0.5r_{LM}^2])r)^2}\right] \\
\times (1 + Cos[2\pi t]\exp[-7r_{LM}])8\pi T\nu.
\end{aligned}
\tag{17}
$$

This parametrization only works for values of $r_{LM} < 2$.

The parametrizations made for $SU(2)$ is then embedded into $SU(3)$ and the random ensemble is generated for 200 different L dyons. The size of the box and the constant r_{LM} is varied, until we obtain a difference in the axial and vector channel that is similar to the experimental results. The results of this fit are shown in Sec. V.

The crucial parameter here and in the previous expression is r_{LM}, in $SU(2)$ the distance between the L and M dyons. Its value used will be explained in the next section.

The correlation functions are given by the Feynman diagrams, in which quark-antiquark pair for mesons, or three quarks for baryons, propagate from x to y. For the quark propagator we use the approximation well developed for the instantons. Its zero mode part has the structure $\langle x|i\rangle(T^{-1})_{ij}\langle j|y\rangle$ where $\langle j|y\rangle = \psi_0(y)$ is the zero mode shifted to the location of the jth dyon. Note that the propagator includes the *inverse* hopping matrix, since the propagator is inverse to the Dirac operator.

For any configuration of the dyons, the set of zero modes are calculated. The 200×200 hopping matrix is filled and inverted. The obtained quark propagator is inserted in all diagrams, convoluted with various matrices in the currrents. The ensemble of configurations we use include 10 configurations.

V. THE CORRELATORS

A. Mesonic correlators

As explained in the Introduction, the difference in the correlation functions for the vector (charged ρ) and axial (charged A_1) channels $V(x) - A(x)$, related to $SU(N_f)$ chiral symmetry breaking, is the most accurately known topology-related combination, both from the experimental inputs and from the lattice. However, it is not the difference corresponding to the largest splitting, which is that between the pseudoscalar and scalar channels.

Let us start to display our results by showing, in Fig. 6, how both the $V(x) - A(x)$ and $P(x) - S(x)$ differences depend on the parameter r_{LM} of our model.
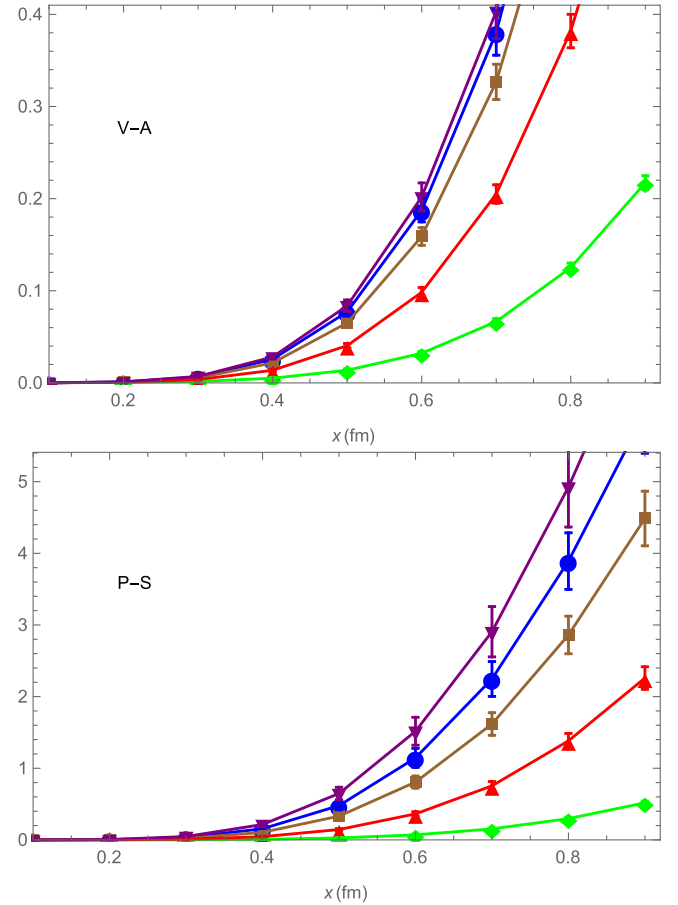

FIG. 6. The upper plot is the difference between the vector and axial correlators $(V(x) - A(x))/(2K_0(x))$ versus the temporal distance x (in fm). The lower plot is the difference between the pseudoscalar and scalar correlators $(P(x) - S(x))/(2K_0(x))$. Different curves are for values of the parameter $r_{LM} = 0.1$ (*Purple*$\triangledown$), 0.15(*Blue*•), 0.2(*Orange*□), 0.3(*Red*△), 0.5(*Green*◇).

The first observation from this figure is that indeed the second $P - S$ splitting is much larger than the first $V - A$, by about one order of magnitude.

The second observation, clearly seen in both of the plots, is that they are quite sensitive to the magnitude of the parameter r_{LM}, the typical distance from the L dyon to the M dyons. By varying it one finds very different magnitude of the correlation functions. Therefore, using this sensitivity we can tune the value of this parameter to correspond to the known vacuum value of the $V - A$ correlator, see Fig. 7. The used value for the fit were $r_{12} = 0.2$.

We see that the fit works well up to distance about $0.5 fm$, but after this overshoots the experimental and lattice data at $|x| > 0.5 fm$. In the latter region one also observes several unphysical effects, in particular the scalar correlator gets negative $S(x) < 0$, see Fig. 7, in contradiction to spectral decomposition which require all diagonal correlation functions to be strictly positive.

These abnormal phenomena in fact have been observed long before, in random instanton liquid model (RILM) and later in quenched QCD [21]. Note that both of these approaches lack the fermionic determinant in the measure, and thus lack the most critical back reaction of quarks on the topological ensemble. Arbitrary operations like "quenching" break connections between these ensembles and quantum field theory foundations, so the correlator positivity and other general features of QFTs can and are violated.

It has been later shown (see the review Schafer:1996wv) that in the so-called interacting instanton liquid model (IILM)—which includes the fermionic determinant in the measure—these abnormal phenomena disappear. And they, of course, also are not present in unquenched lattice simulations with the dynamical quarks. So, although we have not yet done simulations with fully interacting
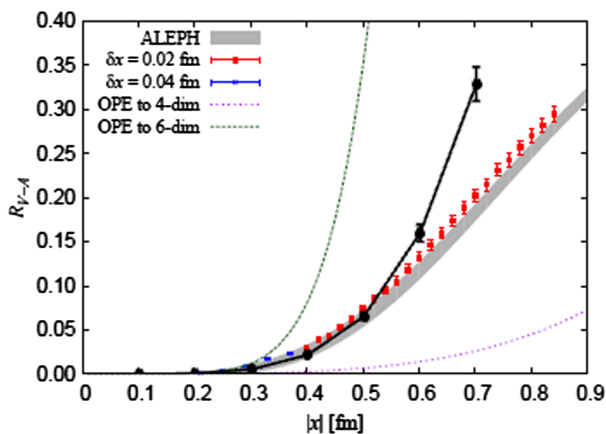
(unquenched) ensemble for SU(3) instanton-dyons, we are confident that in this case these abnormalities would disappear as well.

Now we return to Fig. 8 in which the correlations functions are shown for all four channels under consideration, P, V, A, S from top to bottom. One can clearly see, that for small distances $x < 1/3 fm$ all of them are in a good approximation identical. We further recall that their value in this region, equal to 1 in our normalization, corresponds to free propagation of the massless quark and antiquark.

At larger distances in Fig. 8 our simulations for the four channels display clear splitting pattern, which is nearly identical to what was first observed in RILM and then on the lattice in the 1990s. The lines going upward correspond to attractive channels P, V and those going downward show repulsion in the A, S channels. For comparison we also show in this figure the results from [21], shown by similar symbols as ours but without connecting lines. Overall our results are reasonably well consistent with these lattice data. On a quantitative level one finds certain differences: e.g., the splitting of our pseudoscaler is slightly weaker than on the lattice. All these differences are however completely understandable and are due to different values of the quark masses in our ensemble and on the lattice.

The last subject we would like to discuss for the mesonic correlators is how they change as the temperature increases. These changes are supposed to be caused by (at least) the following effects:

(i) the VEV of the Polyakov line moves toward trivial value 1, and thus the holonomy parameter ν goes towards 0;

(ii) the effective coupling runs to smaller values, the action of the dyons grow and their density decreases;
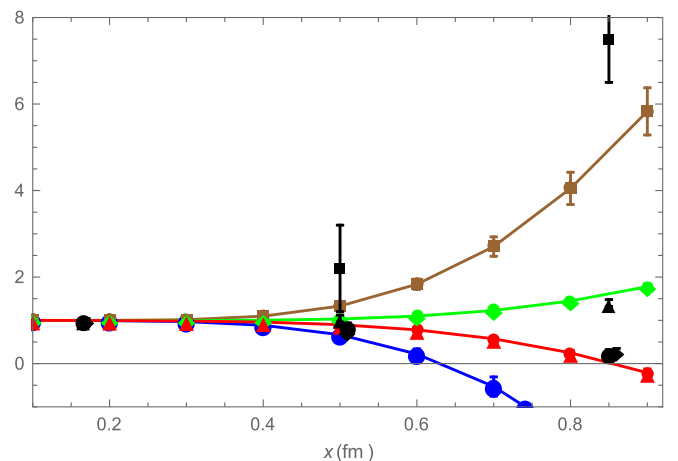
(iii) the size of the Matsubara box decreases.

FIG. 7. The normalized vector minus axial vector difference $(V(x) - A(x))/(2K_0(x))$ channels versus the distance x (fm). The narrow shadowed region corresponds to ALEPH data, the red and blue dots correspond to the lattice data [26], for two lattice spacings indicated on the plot. Our results for $r_{12} = 0.2$ are shown by (black) •).

FIG. 8. The colored points connected by lines are our results for four channels, for $r_{12} = 0.2$. Top to bottom: Pseudoscalar (Brown) □, Vector (Green) ◇, Axial vector (Red) △, and Scalar (Blue) •. The individual (black) points without lines are lattice data from [21], their symbols are the same as for our data.

We implement only the first two modifications, ignoring the last kinematical one and keeping (for illustration purposes) the same box size. The results of the calculations with a modified ensembles are shown in Fig. 9.

Both the $V - A$ and $P - S$ differences of the correlators decrease, as the corresponding modifications are implemented. As expected, such decrease display the tendency of chiral symmetry breaking effects to "melt away" at higher T.

Furthermore, a careful observer would notice that the decrease in the $(V(x) - A(x))$ (upper plot) is much stronger than in the $(P(x) - S(x))$ case (the lower plot). Compare especially the "highest T" points, shown by red triangles.

This means that the restoration of the chiral $SU(N_f)$ symmetry proceeds more rapidly than the restoration of the chiral $U(1)_a$ symmetry. This is indeed what is expected on general grounds [30]: while the former symmetry is broken

spontaneously and gets restored at $T > T_c$, the latter one is broken explicitly by the anomaly and never disappears. If the instanton-dyon ensembles used would be fully "unquenched" from full dynamical simulations including the fermionic determinant, one should see both phenomena directly. Unfortunately, in this first study we use random ensembles only, with not-so-small quark mass, and thus full restoration of the chiral $SU(N_f)$ symmetry, or $V - A = 0$ at $T > T_c$, is not there. Yet it is nice to see that it is at least is getting quite small.

B. Baryonic correlators

Local currents without derivatives with the quantum numbers corresponding to the nucleons (with three flavors, the members of the spin-1/2 $SU(3)_f$ octet) and delta resonance (the members of the spin 3/2 $SU(3)_f$ decuplet) has been defined in [31] and are known as Ioffe currents.

The proton current is

$$J_p = (u^T C d)u - (u^T C \gamma_5 d)\gamma_5 u \qquad (18)$$

where the index T means the transposed spinor and C indicates the charge conjugation: both are needed to write a fermion as an antifermion, to close the bracket (convolute the color and spinor indices). In such notations the current color and spinor indices (not shown) are those of the last quark.

The delta has a current of a single simple structure, e.g., the charge 3/2 one

$$J_\Delta = (u^T C \gamma_\mu u)u \qquad (19)$$

and 4 correlators, two "nonflip" and two "flip" ones.

We had explained the color structure of the correlators, but not yet the spinor one. Each correlator defined above has two currents which are spinors: so one can sandwich in any gamma matrix and take the trace. Physically, there are two possible spin structures for the nucleon, with and without a spin flip of the nucleon, corresponding to choices $\mathrm{Tr}[K]$, $\mathrm{Tr}[\gamma_0 K]$. Since one can also study any nondiagonal correlators, there are in total 6 correlations functions for the nucleon. Two of them are "nonflip" and must tend to 1 at small distances, the others go to zero there. The delta current has only one color structure but more possible spin transitions, so in total there are 4 functions.

Results from our simulations for these ten correlation functions are displayed in Fig. 10 and Fig. 11 respectively. The normalization is similar to that in the previous subsection, but now to the propagation of *three* free massless quarks $K_0 \sim 1/|x|^9$. Note that variation of different correlators in this normalization is not very drastic, although in absolute normalization the correlators would change by about 10^9 over the range of this plot.

Like for mesonic correlators, we also compare the results for some nucleon and delta correlators to the available
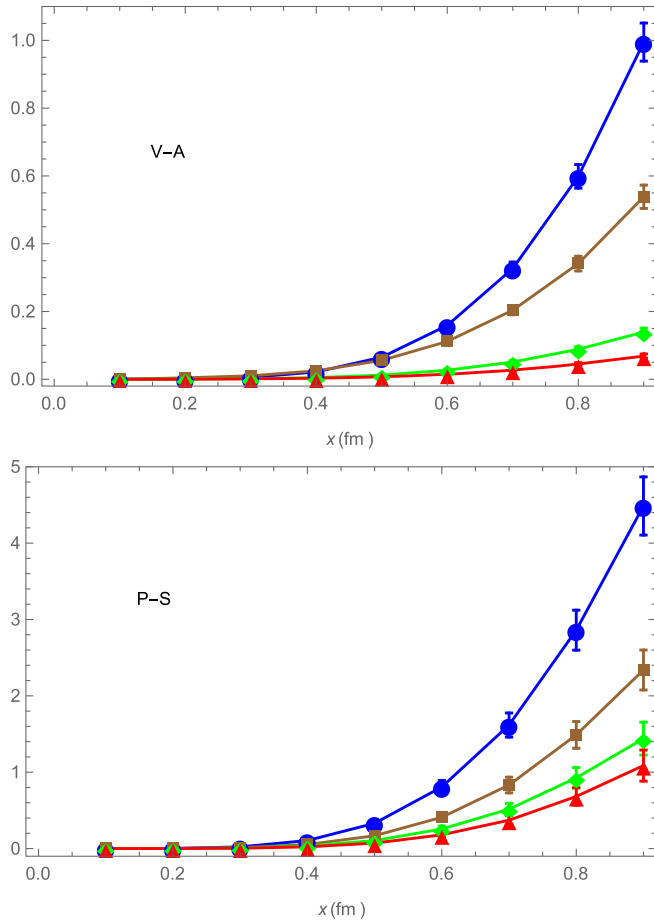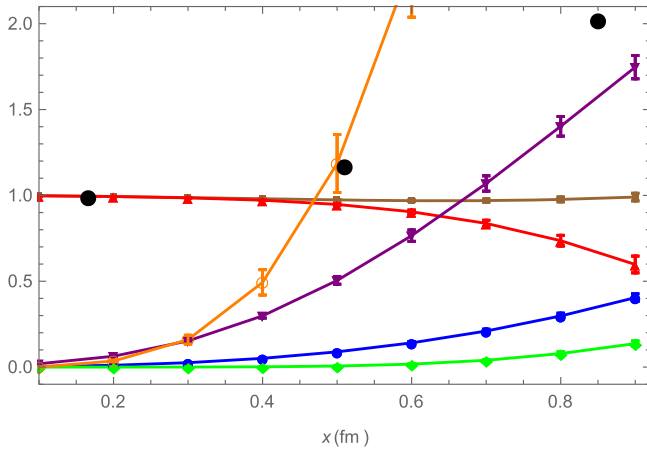

FIG. 9. The upper plot is the difference between the vector and axial correlators $(V(x) - A(x))/(2K_0(x))$ versus the temporal distance x (in fm). The lower plot is the difference between the pseudoscalar and scalar correlators $(P(x) - S(x))/(2K_0(x))$. $r_{LM} = 0.2$. Different curves are for values of the density and holonomy: $\nu = 1/3$, $n = 0.8$ blue closed circle •; $\nu = 1/6$, $n = 0.8$ brown box □; $\nu = 1/6$, $n = 0.46$ green diamond ◇; $\nu = 1/6$, $n = 0.29$ red triangles △.

FIG. 10. All six nucleon correlators, see text, versus the distance $x(fm)$, for $r_{12} = 0.2$. The individual black points without line are lattice data from [21]. Those should be compared to the lines with the same symbol.

lattice data from [21], shown by points without connecting lines, and corresponding to quenched quark simulation.

As we already mentioned, the main difference between the nucleon (spin-1/2 octet baryons) and the Delta (spin-3/2 decuplet baryons) is due to the fact that the former includes "good" spin-0 diquark, while the latter has "bad" spin-1 diquark. The former one is deeply bound, due mainly to the operator of the topological origin, the 't Hooft Lagrangian.

Already in [20] it has been proposed to look at heavy-light correlation functions, made of a static quark plus the diquarks. The one of interest is the Λ-type

$$K_\Lambda(x) = \left\langle (J_\Lambda(x))_n^+ P \exp\left[\frac{ig}{2}\int_0^x A_\mu^a t^a dx^\mu\right]_{nk} (J_\Lambda(0))_k \right\rangle$$

including the "good diquark" current $J_\Lambda(x)_k = u_i^T(x)C\gamma_5 d_j(x)\epsilon_{ijk}$. (For "bad" diquark the current can

be modified by the substitution $\gamma_5 \to \gamma_\mu$.) Note that we have explicitly shown here the color indices, to emphasize the fact that any diquark has spin-color quantum number of an antiquark. In order to make the correlator gauge invariant one needs to include the connector, the path order exponent, from one point to another.

Before showing our numerical results for the diquark correlator, two comments are in order. One is that in a particular case of $SU(2)$ color group this diquark is a colorless baryon, degenerate with the pion due to Pauli-Gurcey symmetry. While our calculations are for the $SU(3)$, in which no such symmetry is present, one still may expect certain continuity in N_c and thus a strong attraction in this channel. The second, following from the first, is that the "good" (ud spin-0) diquark is the most attractive channel, thus leading to phenomenon of color superconductivity at high density.

In Fig. 12 we show our measurements of this correlation function. We use an approximation $P \exp[(ig/2) \times \int_0^x A_\mu^a t^a dx^\mu] \approx 1$ since its evaluation on our model is expensive—one needs to calculate the gauge fields from all the dyons along the straight line from x to y—and rather unimportant numerically. As one can see from this figure, the normalized correlator goes upward with an increasing distance. Since the normalization is to the free quark propagation, such behavior indicate attraction between quarks in this channel.

Its magnitude is roughly consistent with what was observed in the instanton liquid model [32]. There is a simple explanation of its magnitude, based on the analytically known dependence of the 't Hooft Lagrangian on the number of colors: the factor in the qq channel relative to $\bar{q}q$ follows from Fierz transformation and is $f_{N_c} = 1/(N_c - 1)$. Note that at $N_c \to \infty$ one has
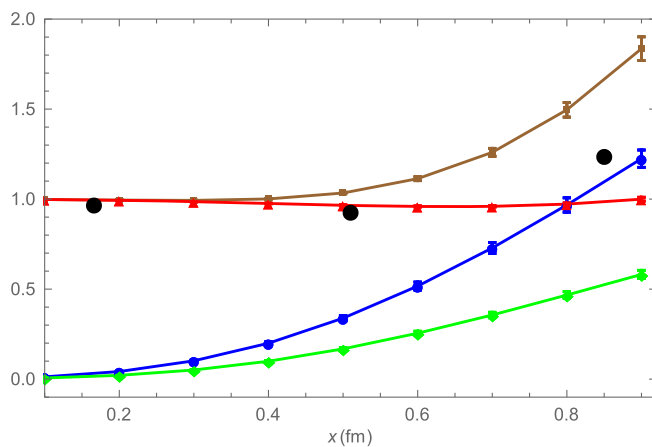

FIG. 11. All four delta correlators versus the distance $x(fm)$, for $r_{12} = 0.2$. The black closed points without lines are lattice data [21]. Those should be compared to the lines with the same symbol.
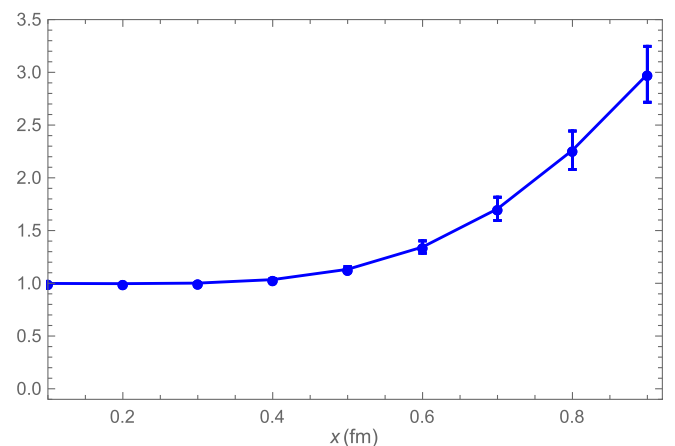

FIG. 12. The normalized correlator for a "good" (ud spin-0) diquark channel versus distance $x(fm)$. As other plots, it is done for ensemble of correlated $L - M$ dyons with $r_{12} = 0.2$, in a box of size $2fm$ in time direction and $5fm$ in spatial directions, with 200 zero-modes, which gives a density of $0.8fm^{-4}$.

$f_{N_c} \to 0$. At $N_c = 2$ one finds $f_2 = 1$, consistent with Pauli-Gurcey symmetry. For the case of QCD and our simulations $N_c = 3$, thus the relevant factor is $f_3 = 1/2$. It is gratifying to see that the simulation results for the diquark show splitting from 1 being indeed roughly a half of what is observed in the pion channel.

VI. SUMMARY AND DISCUSSION

By this paper we started studies of the hadronic correlation functions at nonzero temperatures T, using numerically generated ensembles of the instanton-dyons. Specifically, in it we addressed the question whether this version of the semiclassical theory, at its lowest range of applicability $T \approx T_{\min} \sim 100$ MeV, can or cannot correctly reproduce many important nonperturbative phenomena in the QCD vacuum. More specifically, we have done so by explicit evaluation of multiple mesonic and baryonic two-point correlation functions.

The instanton liquid model has demonstrated successful description of those already in the 1990s, and thus one might naively think that the instanton-dyon ensemble would easily reproduce these functions as well, provided the density n_L (per the dyon type) be in the ballpark of the instanton density $n_{\text{inst}} \sim 1 fm^{-4}$.

What we have found is that this task is by no means trivial or even simple to fulfill. The reason is the main element of the calculation, the quark zero modes, are in fact very different for the dyons and instantons. The dyons are natural at high T, at which the temporal extent of the Matsubara box $\beta = 1/T$ is small, one therefore one can reduce the 4-d theory to its 3-d approximation. The sizes of the individual dyons are fixed by the β and are small at high T.

However at low T the dyon sizes are getting comparable to the interparticle distances, or even exceed those. If so, the dyons start to overlap, partially screening each other. A close pair of LM dyons (in SU(2)) or triplets LM_1M_2 (in SU(3)) cancel the fields except in a small central core. Yet, the topological charge is *not* screened, and the index theorems thus guarantee the existence of quark zero modes. As those are localized stronger, to a smaller volume, their normalization condition forces them to become locally very strong. As seen in Sec. III, their density grows by about two orders of magnitude.

Since the nontrivial part of the correlation functions of (gauge invariant) currents depend on local density of these zero modes, one also observes a very strong dependence of those on the dyon correlation parameter r_{LM}.

Using accurately known $V - A$ correlator, we were able to tune the value of this parameter to r_{LM} to it. After this is done, we calculate several other correlators as well.

Of particular importance are two strongest effects of the topological origin:
  (i) the $P - S$ or $\vec{\pi} - \vec{\delta}$ splitting, violating the $U(1)_a$ chiral symmetry, and

  (ii) the *ud* quark pairing into the "good diquark," present inside the nucleons. hadronic phenomenology.

Finally, let us recall that—both on the lattice and in the semiclassical instanton-dyon theory—there remains to study how all the correlation functions and the particular splitting effects we studied above depend at the temperature. The $V - A$ combination should vanish for massless quarks at $T > T_c$, as the $SU(N_f)$ chiral symmetry gets restored. (Or be $O(m)$ if the quark mass is nonzero.) The other—and larger—splitting $\vec{\pi} - \vec{\delta}$ is expected to be nonzero at any T, as the $U(1)_a$ chiral symmetry never gets restored. While our random "quenched" ensemble does not fully display this difference, as we have shown above, it does show it approximately.

Let us emphasize the importance of high accuracy lattice studies of the issues involved. This task has recently been carried out (for vector and axial isovector channels) in Ref. [26], showing good agreement with phenomenology and with the calculation in the framework of the instanton liquid model [25]. Such studies should be extended to the finite temperatures. While hadrons themselves "melt" at high temperatures, get large widths and eventually completely disappear in hot quark-gluon plasma, the correlation functions of gauge-invariant operators are well-defined at any temperatures, and therefore they are the main observables, studied in lattice gauge theory and hadronic phenomenology.

Our paper is based on an ensemble of the instanton-dyons, which has confinement at $T < T_c$. So we expect the near-realistic spectrum, improved compared to instanton-based calculations of the 1990s. At the other hand, in this pilot "quenched" study, we use ensembles with randomly populated dyons. We expect to do full dynamical calculations in subsequent works, and see how the correlators would be affected.

One important issue we would like to understand in those works, by a comparison of the results of this work with phenomenology, is the issue of "rigid breaking" of the color group $SU(3) \to U(1)^2$. The nonzero holonomy phenomenon, well studied on the lattice, is $\langle P(T) \rangle \neq 1$. This function provide a *local* (in $\bar{x}$) representation of the *trace* of the unitary operator, which we parametrize in terms of its eigenvalues μ_i, which are the main building blocks of the instanton-dyon model.

The residual local $SU(3)$ rotations do not change the $\langle P(T) \rangle$ eigenvalues and the instanton-dyon actions. Thus they are irrelevant for the noninteracting dyon ensemble we use. But they are relevant for the quark propagators used. Indeed, a quark propagating from a dyon located at point x to the dyon located at point y finds two different sets of zero modes at x and y, rotated by this residual local $SU(3)$ transformations differently. We do not have much first-principle information on the correlation length of these residual local $SU(3)$ rotations, and therefore approach the issue on

try-and-see phenomenological bases. Therefore we will compare two limiting cases:

    (i) a *"rigid breaking"* of $SU(3) \rightarrow U(1) \times U(1)$", in which the eigenvectors of the Polyakov line have the same direction everywhere, and thus all dyons have the same color orientation; and

    (ii) *"random breaking,"* in which all dyons are rotated randomly by independent $SU(3)$ matrices.

[1] A. A. Belavin, A. M. Polyakov, A. S. Schwartz, and Y. S. Tyupkin, Pseudoparticle solutions of the Yang-Mills equations, Phys. Lett. **59B,** 85 (1975).

[2] E. V. Shuryak, The role of instantons in quantum chromodynamics. 1. Physical vacuum, Nucl. Phys. **B203,** 93 (1982).

[3] Y. Nambu and G. Jona-Lasinio, Dynamical model of elementary particles based on an analogy with superconductivity. 1., Phys. Rev. **122,** 345 (1961).

[4] T. Schafer and E. V. Shuryak, Instantons in QCD, Rev. Mod. Phys. **70,** 323 (1998).

[5] T. C. Kraan and P. van Baal, Monopole constituents inside SU(n) calorons, Phys. Lett. B **435,** 389 (1998).

[6] K. M. Lee and C. H. Lu, SU(2) calorons and magnetic monopoles, Phys. Rev. D **58,** 025011 (1998).

[7] N. M. Davies, T. J. Hollowood, V. V. Khoze, and M. P. Mattis, Gluino condensate and magnetic monopoles in supersymmetric gluodynamics, Nucl. Phys. **B559,** 123 (1999).

[8] D. Diakonov, Topology and confinement, Nucl. Phys. B, Proc. Suppl. **195,** 5 (2009).

[9] E. Poppitz and M. Unsal, Seiberg-Witten and Polyakov-like' magnetic bion confinements are continuously connected, J. High Energy Phys. 07 (2011) 082.

[10] E. Poppitz, T. Schfer, and M. Unsal, Continuity, deconfinement, and (super) Yang-Mills theory, J. High Energy Phys. 10 (2012) 115.

[11] Y. Liu, E. Shuryak, and I. Zahed, Confining dyon-antidyon Coulomb liquid model. I., Phys. Rev. D **92,** 085006 (2015).

[12] Y. Liu, E. Shuryak, and I. Zahed, Light quarks in the screened dyon-antidyon Coulomb liquid model. II., Phys. Rev. D **92,** 085007 (2015).

[13] Y. Liu, E. Shuryak, and I. Zahed, The instanton-dyon liquid model III: Finite chemical potential, Phys. Rev. D **94,** 105011 (2016).

[14] Y. Liu, E. Shuryak, and I. Zahed, Light adjoint quarks in the instanton-dyon liquid model IV, Phys. Rev. D **94,** 105012 (2016).

[15] Y. Liu, E. Shuryak, and I. Zahed, The instanton-dyon liquid model V: Twisted light quarks, Phys. Rev. D **94,** 105013 (2016).

[16] P. Faccioli and E. Shuryak, QCD topology at finite temperature: Statistical mechanics of self-dual dyons, Phys. Rev. D **87,** 074009 (2013).

[17] R. Larsen and E. Shuryak, Interacting ensemble of the instanton-dyons and the deconfinement phase transition in the SU(2) gauge theory, Phys. Rev. D **92,** 094022 (2015).

[18] R. Larsen and E. Shuryak, Instanton-dyon ensemble with two dynamical quarks: The chiral symmetry breaking, Phys. Rev. D **93,** 054029 (2016).

[19] R. Larsen and E. Shuryak, Instanton-dyon ensembles with quarks with modified boundary conditions, Phys. Rev. D **94,** 094009 (2016).

[20] E. V. Shuryak, Correlation functions in the QCD vacuum, Rev. Mod. Phys. **65,** 1 (1993).

[21] M. C. Chu, J. M. Grandy, S. Huang, and J. W. Negele, Lattice Calculation of Point-to-Point Hadron Current Correlation Functions in the QCD Vacuum, Phys. Rev. Lett. **70,** 255 (1993).

[22] M. A. Shifman, A. I. Vainshtein, and V. I. Zakharov, QCD and resonance physics. theoretical foundations, Nucl. Phys. **147,** 385 (1979); QCD and resonance physics. applications, Nucl. Phys. **147,** 448 (1979); QCD and resonance physics: The $\varrho - \omega$ mixing, Nucl. Phys. **147,** 519 (1979).

[23] R. Barate *et al.* (ALEPH Collaboration), Measurement of the spectral functions of vector current hadronic tau decays, Z. Phys. C **76,** 15 (1997).

[24] R. Barate *et al.* (ALEPH Collaboration), Measurement of the spectral functions of axial—vector hadronic tau decays and determination of alpha(S)(M**2(tau)), Eur. Phys. J. C **4,** 409 (1998).

[25] T. Schafer and E. V. Shuryak, Implications of the ALEPH Tau Lepton Decay Data for Perturbative and Nonperturbative QCD, Phys. Rev. Lett. **86,** 3973 (2001).

[26] M. Tomii *et al.* (JLQCD Collaboration), Lattice calculation of vector and axial-vector current correlators in QCD, arXiv:1703.06249.

[27] P. Faccioli and T. A. DeGrand, Evidence for Instanton Induced Dynamics, from Lattice QCD, Phys. Rev. Lett. **91,** 182001 (2003).

[28] E. Shuryak and T. Sulejmanpasic, The chiral symmetry breaking/restoration in dyonic vacuum, Phys. Rev. D **86,** 036001 (2012).

[29] F. Bruckmann, D. Nogradi, and P. van Baal, Constituent monopoles through the eyes of fermion zero modes, Nucl. Phys. **B666,** 197 (2003).

[30] E. V. Shuryak, Which chiral symmetry is restored in hot QCD?, Comments Nucl. Part. Phys. **21,** 235 (1994).

[31] B. L. Ioffe, Calculation of baryon masses in quantum chromodynamics, Nucl. Phys. **B188,** 317 (1981); Erratum, Nucl. Phys. **B191,** 591 (1981).

[32] T. Schafer, E. V. Shuryak, and J. J. M. Verbaarschot, Baryonic correlators in the random instanton vacuum, Nucl. Phys. **B412,** 143 (1994).